The Extraordinary Specificity of Xanthine Phosphoribosyltransferase from *Bacillus subtilis* Elucidated by Reaction Kinetics, Ligand Binding, and Crystallography[†,‡]

Susan Arent,[§,||] Anders Kadziola,[§] Sine Larsen,[§,⊥] Jan Neuhard,[#] and Kaj Frank Jensen*[,#]

Centre for Crystallographic Studies, Department of Chemistry, University of Copenhagen, Universitetsparken 5, DK-2100 Copenhagen Ø, Denmark, European Synchrotron Radiation Facility, B.P. 220, 38043 Grenoble, France, and Department of Biological Chemistry, Institute of Molecular Biology, University of Copenhagen, Sølvgade 83H, DK-1307 Copenhagen K, Denmark

Received February 10, 2006

ABSTRACT: Xanthine phosphoribosyltransferase (XPRTase) from *Bacillus subtilis* is a representative of the highly xanthine specific XPRTases found in Gram-positive bacteria. These XPRTases constitute a distinct subclass of 6-oxopurine PRTases, which deviate strongly from the major class of H(X)GPRTases with respect to sequence, PRPP binding motif, and oligomeric structure. They are more related with the PurR repressor of Gram-positive bacteria, the adenine PRTase, and orotate PRTase. The catalytic function and high specificity for xanthine of *B. subtilis* XPRTase were investigated by ligand binding studies and reaction kinetics as a function of pH with xanthine, hypoxanthine, and guanine as substrates. The crystal structure of the dimeric XPRTase−GMP complex was determined to 2.05 Å resolution. In a sequential reaction mechanism XPRTase binds first PRPP, stabilizing its active dimeric form, and subsequently xanthine. The XPRTase is able also to react with guanine and hypoxanthine albeit at much lower (10^{-4}-fold) catalytic efficiency. Different pK_a values for the bases and variations in their electrostatic potential can account for these catalytic differences. The unique base specificity of XPRTase has been related to a few key residues in the active site. Asn27 can in different orientations form hydrogen bonds to an amino group or an oxo group at the 2-position of the purine base, and Lys156 is positioned to make a hydrogen bond with N7. This and the absence of a catalytic carboxylate group near the N7-position require the purine base to dissociate a proton spontaneously in order to undergo catalysis.

Xanthine phosphoribosyltransferase (XPRTase) from the spore forming Gram-positive bacterium *Bacillus subtilis* catalyzes the formation of the nucleotide XMP (and pyrophosphate) from the purine base xanthine and the phosphoribosyl donor 5-phosphoribosyl-α-1-diphosphate (PRPP[1]). The enzyme belongs to the greater class of phosphoribosyltransferases (type 1 PRTases), which are ultimately responsible for formation of the linkage between the base and pentose moieties in all nucleotides because they participate in the biosynthesis of purine and pyrimidine nucleotides by both de novo and salvage pathways (*1*). The salvage pathways convert preformed bases and nucleosides to nucleotide level so that these compounds, stemming from breakdown of nucleic acids, may be reused for RNA and DNA synthesis. XPRTase is part of the purine salvage pathway. In general, organisms contain two types of purine PRTases, namely, an APRTase which is highly specific for adenine (i.e. 6-amino-purine) and one or more 6-oxo-purine PRTases that use one or more of the 6-oxo-purines (hypoxanthine, xanthine, or guanine, see Figure 1) as substrates (*2*, *3*). Most PRTases, like the human HGPRTase (*4*), that are able to use hypoxanthine and/or guanine as substrates discriminate against xanthine, which deviates from the other 6-oxo-purines (hypoxanthine and guanine) by virtue of its negative charge at neutral pH. The purine base, xanthine, dissociates a proton with a pK_a equal to 7.7, and the nucleotide product, XMP, is highly acidic, pK_a = 5.7 (*5*). Some 6-oxo-purine PRTases, however, are able to use xanthine on equal terms with other 6-oxo-purines, exemplified by the HGXPRTase from *Toxoplasma gondii* (*6*−*8*) and the xanthine−guanine PRTase

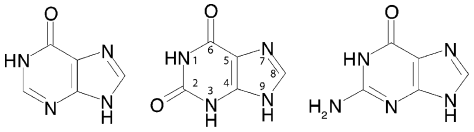

FIGURE 1: Schematic drawings of xanthine, guanine, and hypoxanthine.

[†] This work was supported by grants from the Danish National Research Foundation and the Faculty of Science, University of Copenhagen, and the EU subprogram Access to Research Infrastructures.

[‡] Coordinates of the structure of xanthine phosphosphoribosyltransferase have been deposited in the Protein Data Bank under ID 2FXV.

* To whom correspondence should be addressed. Tel: +45 3532 2020. Fax: +45 3532 2040. E-mail: kfj@mermaid.molbio.ku.dk.

[§] Department of Chemistry, University of Copenhagen.

[||] Present address: Carlsberg Laboratory, Gamle Carlsberg Vej 10, DK-2500 Valby, Denmark.

[⊥] European Synchrotron Radiation Facility.

[#] Institute of Molecular Biology, University of Copenhagen.

[1] Abbreviations: PRPP, 5-phosphoribosyl-1-α-diphosphate; PP_i, inorganic diphosphate; GMP, guanosine 5′-monophosphate; IMP, inosine 5′-monophosphate; XMP, xanthosine 5′-monophospate; IPTG, isopropyl-β-D-thiogalactoside; GdHCl, guanidinium hydrochloride; PRTase, phosphoribosyltransferase; APRTase, adenine PRTase; HPRTase, hypoxanthine PRTase; XPRTase, xanthine PRTase (EC 2.4.2.22); PurR, purine repressor protein; buffer A, 25 mM Tris-HCl−0.1 mM EDTA pH 7.6; PCR, polymerase chain reaction.

10.1021/bi060287y CCC: $33.50
Published on Web 05/03/2006

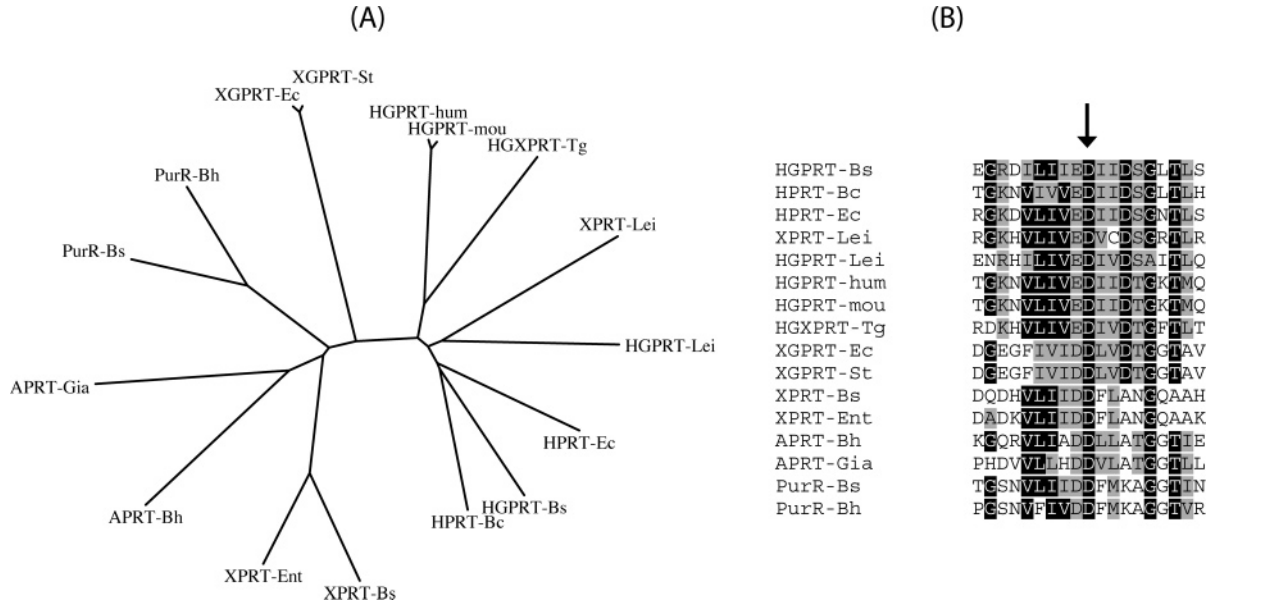

FIGURE 2: Evolutionary relationship between different purine PRTases and the purine repressor (PurR). The sequences were chosen as typical representatives of the different functional families of PRTases and aligned using the program CLUSTALW (*19*). The unrooted tree (panel A) was made according to Felsenstein (*20*). The PRPP motifs from the aligned sequences are shown in panel B. The fully conserved aspartate in the PRPP motif, marked with an arrow, is residue D125 in *B. subtilis* XPRTase. Abbreviations: XPRT-Bs, *B. subtilis* enzyme; XPRT-Ent, enzyme from *E. faecalis*; APRT-Bh, enzyme from *Bacillus halodurans*; APRT-Gia, enzyme from *G. lambia*; PurR-Bh, repressor protein from *B. halodurans*; PurR-Bs, repressor protein from *B. subtilis*; XGPRT-Ec, enzyme from *E. coli*; XGPRT-St, enzyme from *Salmonella typhimurium*; HGPRT-hum, enzyme from human; HGPRT-mou, enzyme from mouse; HXGPRT-Tc, enzyme from *T. gondii*; XPRT-Lei, enzyme from *L. donovani*; HGPRT-Lei, enzyme from *L. donovani*; HPRT-Ec, enzyme from *E. coli*; HGPRT-Bs, enzyme from *B. subtilis*; HPRT-Bc, enzyme from *Bacillus cereus*.

(GXPRTase) of *Escherichia coli* (*9*). Some of these, including the xanthine-preferring PRTase from *Leishmania donovani* (*10*, *11*), have previously been termed xanthine phosphoribosyltransferases. The XPRTase of *B. subtilis* described in this work exhibits, however, an unusually high specificity for xanthine and a strong discrimination against hypoxanthine and guanine as substrates, which only seems to be matched by the similar enzyme from *Enterococcus faecalis* studied years ago (*12*). The XPRTases also deviate in sequence from most other 6-oxo-purine PRTases by being more related in sequence to the adenine PRTases and the purine repressor protein of Gram-positive bacteria (Figure 2A), which also contains a PRTase domain (*13*). The highly specific nature of XPRTase from *B. subtilis* was recognized by finding that mutants, which lacked the *hpt* gene encoding HGPRTase, but carried a functional the *xpt* gene encoding XPRTase, were unable to satisfy their purine requirement with exogenous purine bases other than xanthine (*14*).

All type 1 PRTases share a common fold, which was first observed and described for the orotate phosphoribosyltransferase from *Salmonella typhimurium* (*15*). They carry a shared sequence motif, termed the PRPP motif (*16*, *17*), which binds the 5-phosphoribosyl moiety of PRPP and the nucleotide product. In all cases, except for the highly specific uracil phosphoribosyltransferases, the PRPP binding motif contains two adjacent acidic residues which are involved in contacts with the vicinal hydroxyl groups of the ribose phosphate moiety. In the major class of H(X)GPRTases the two acidic residues are a glutamate followed by an aspartate (*18*), but the XPRTases of Gram-positive bacteria like *B. subtilis* and *E. faecalis* contain two consecutive aspartate residues. Figure 2B shows the aligned sequences of the PRPP motifs of a selected set of PRTases including also two representatives of the PurR repressor protein of Gram-positive bacteria. It is clear that the PRPP motif of XPRTase like the full sequences is more related to the APRTases and the PurR proteins than to most of the 6-oxo-purine PRTases.

The unusual amino acid sequence and its sequence similarity to proteins other than the HGXPRTases inspired our investigations of the extraordinarily high specificity of the *B. subtilis* XPRTase for xanthine. To examine this in greater detail a high yielding expression system in *E. coli* of the protein was constructed that gave sufficient quantities for the subsequent kinetic and ligand binding studies. Surprisingly the enzyme proved to be fully saturated with GMP when extracted from *E. coli*. This observation prompted a more detailed investigation of the substrate specificity and determination of the crystal structure of the enzyme−GMP complex. Combining the results from the structural and kinetic data, we have been able to present here an explanation of parts of the unique xanthine specificity displayed by the *B. subtilis* XPRTase.

MATERIALS AND METHODS

Materials. The radiochemicals [8-^{14}C]XMP, [8-^{14}C]GMP, and [8-^{14}C]IMP were purchased from Moravek Biochemicals (CA). [8-^{14}C]-Labeled purine bases (adenine, hypoxanthine, guanine, and xanthine), [γ-^{32}P]ATP, and [^{32}P]pyrophosphate were from NEN Life Science Products. [^{32}P]PRPP was prepared from [γ-^{32}P]ATP and ribose-5-phosphate as previously described using *E. coli* PRPP synthetase to catalyze the reaction (*21*). Unlabeled nucleotides and purine bases were bought from Sigma. Guanidinium hydrochloride and other fine chemicals were from Sigma, Serva, Merck, Calbiochem, or Baker. The BigDye Terminator Cycle Sequencing v2.0 Ready Reaction kit with AmpliTaq polymerase for the ABI Prism sequencing apparatus was from

PE Biosystems (CA). Yeast alcohol dehydrogenase was from Boehringer. *E. coli* orotate phosphoribosyltransferase was prepared as described (*22*). *E. coli* PRPP synthase was a gift from Dr. Martin Willemoës (University of Copenhagen). Synthetic DNA oligonucleotides were bought from DNA Technology A/S, Aarhus, Denmark. Poly(ethyleneimine)-impregnated cellulose thin-layer plates were made according to a described procedure (*23*). Dyematrex Gel Red A was from Millipore Corporation (MA). Sephacryl S-200, a Superose 12 column, and prepacked 10 mL Sephadex G25 (PD10) columns were from Pharmacia Biotech (Uppsala, Sweden). Diethylaminoethyl cellulose (DE52, preswollen) was from Whatman International Ltd. (Maidstone, Kent, England). The bacterial strain NF1830, *E. coli* K-12 (*recA1/F′laI*^{q1} *lacZ::*Tn*5*), has been described before (*24*). Plasmid pSS9 carrying the *B. subtilis xpt* gene (*14*) was a gift from Dr. H. H. Saxild (The Technical University of Denmark).

Construction of an Expression Vector. The expression vector pBSxpt was constructed in the following way. The *xpt* gene on plasmid pSS9 (*14*) was amplified by PCR using the following primers: 5′BSxpt 5′CGCGGATCCGGAGGTAGACAGG*ATGCAAGC* and 3′BSxpt 5′GGAAGCTTCATGAATGAACCTCCTGTA. The PCR product was digested with *Bam*HI and *Hin*dIII and cloned into the plasmid pUHE23-2, which was also digested with *Bam*HI and *Hin*dIII and treated with alkaline phosphatase to prevent self-ligation. This brings transcription of the *xpt* gene under control of the strong $P_{A1/O4/O3}$ promoter (*25*). The resulting plasmid pBSxpt was transformed into strain NF1830 that overproduces the *lac* repressor, so that *xpt* expression was kept repressed until induction by isopropyl-β-D-thiogalactoside (IPTG) (*24*). A derivative of the *xpt* gene encoding a protein with six histidine residues attached to the C-terminus was constructed similarly by PCR using the primer 3′BSxptCHis with the sequence 5′GGAAGCTTCAATGGTGATGGTGATGGTGTGAATGAACCTCCTGTACGAAGG in combination with the 5′BSxpt primer. The amplified DNA fragment was cloned into pUHE23-2 generating the expression plasmid pBSxptCHis. DNA sequencing showed that the *xpt* genes on plasmids pBSxpt and pBSxptCHis had the expected nucleotide sequences (*14*).

Cell Growth. Two liter LB-broth cultures (*26*) of NF1830 transformed with either pBSxpt or pBSxptCHis were grown with vigorous aeration at 37 °C. IPTG (0.5 mM) was added at $OD_{438} = 0.5$ to induce transcription of the *xpt* gene on the plasmid. Growth was continued to reach stationary phase overnight. Cells were harvested by centrifugation and stored frozen at −20 °C.

Purification of Native Xanthine Phosphoribosyltransferase. Initial Steps. Wet cell paste (7 g) of NF1830-pBSxpt was suspended in 40 mL of 0.1 M Tris-HCl pH 7.6−2 mM EDTA and disrupted by ultrasonic treatment. Cell debris was removed by centrifugation. Nucleic acid was precipitated by addition of 1% of streptomycin sulfate and stirring for an hour (6 °C). The extract was cleared by centrifugation and dialyzed for 2 h against 1 L of 25 mM Tris-HCl−0.1 mM EDTA pH 7.6 (buffer A). The protein was applied to a column (1 cm^2 × 20 cm) packed with DEAE-cellulose (DE52). The column was washed with 50 mL of buffer A, and, subsequently, the enzyme was eluted with a 200 mL of linear NaCl-gradient (0.05−0.5 M) in buffer A. Five fractions (10 mL each) containing the enzyme, as revealed by SDS−PAGE, were pooled. Protein was precipitated by addition of solid ammonium sulfate to 80% saturation. After stirring (at 6 °C), the precipitate was collected by centrifugation and dissolved in 50 mL of buffer A. It appeared that the protein at this stage contained substantial amounts of GMP (vide infra). Hence, the ammonium sulfate precipitation procedure was repeated twice. The pellet obtained after the third precipitation was redissolved in a small volume and dialyzed against 1 L of buffer A for 1 h. Following removal of turbidity by centrifugation the protein was passed through a column (5 cm^2 × 85 cm) of Sephacryl S-200 (Pharmacia) equilibrated with buffer A at a pump rate of 1 mL/min while 5 mL fractions were collected. Fractions containing XPRTase were pooled (volume 40 mL). Analysis by SDS−PAGE revealed that the XPRTase after this step was more than 75% pure and that it had lost most of the GMP that it contained after extraction. To obtain homogeneous preparations of XPRTase either free of nucleotide or saturated with GMP or XMP the purification was continued in three different ways (A, B, and C) as described below.

A. Preparation of Nucleotide Free XPRTase. The enzyme as it appeared from the Sephacryl S-200 column was applied to a column of DyeMatrex Gel Red A (10 mL) equilibrated with buffer A. A small fraction of XPRTase, which still contained GMP, passed through the column during application and washing with buffer A and was discarded. The nucleotide free XPRTase (more than 90% homogeneous) was eluted with a linear NaCl-gradient (0−1.0 M) in buffer A. The fractions were concentrated by use of the Centriprep YM-10 device and dialyzed against buffer A.

B. Preparation of the XPRTase−GMP Complex. The nucleotide free enzyme was applied to a column of DyeMatrex Gel Red A (10 mL) equilibrated with buffer A. After washing with buffer A, the enzyme was eluted as a homogeneous peak with 40 mL of buffer A containing 1 mM GMP while fractions were collected. The fractions containing XPRTase were pooled (28 mL) and concentrated to 4.5 mL by use of the Centriprep YM-10 device, dialyzed first against 0.5 L of buffer A and finally against 0.25 L of buffer A containing 12 μM GMP. After this step the concentration of GMP was ≥550 μM inside the dialysis bag and 26 μM in the dialysate. SDS−PAGE analysis revealed an almost 100% homogeneous preparation of XPRTase after this procedure.

C. Preparation of the XPRTase−XMP Complex. The nucleotide free enzyme was applied to a column of DyeMatrex Gel Red A (10 mL) equilibrated with buffer A. After washing with buffer A, the enzyme was eluted as a homogeneous peak with 40 mL of buffer A containing 1 mM XMP while fractions were collected. The fractions containing XPRTase were pooled, precipitated with 80% ammonium sulfate, and desalted by passage through a PD10 column dialyzed overnight against buffer A containing 25 μM XMP. Following dialysis the concentration of XMP outside the dialysis bag was 17 μM and ca. 300 μM inside the dialysis bag. The protein appeared homogeneous according to SDS−PAGE analysis.

Storage and Usage. According to activity measurements, the crude extract of cells from 2 L cultures contained approximately 500 mg of XPRTase. The yield of homogeneous enzyme was around 20% (ca. 100 mg). The enzyme preparations were stored at −20 °C in buffer A containing

50% glycerol and did not show any loss of activity during two years. If instead the enzyme was stored without glycerol at 4 °C it gradually jellified and precipitated. The nucleotide free preparation of XPRTase was used for all kinetic analyses and ligand binding assays. For these purposes, glycerol was removed by passage through a Sephadex G-25 column (PD10) equilibrated with buffer A. The desalted preparations were used on the same day, since the activity and the number of ligand binding sites decayed with a half-life of 4 days during storage at 4 °C.

Purification of C-Terminally Tagged XPRTase. An LB-broth culture (0.5 L) of NF1830 transformed with plasmid pBSxptCHis was grown, induced with IPTG, and harvested as described above. The cells were suspended in 50 mL of 50 mM sodium phosphate pH 8 containing 20 mM imidazole and 0.15 M NaCl and disrupted by ultrasonic treatment. Debris was removed by centrifugation, and the extract was applied to a 5 mL column of NiCAM HC Resin equilibrated with the same buffer. The column was washed with 5 × 5 mL of this buffer, and the His-tagged XPRTase was eluted from the column by washing with 4 × 5 mL of 50 mM sodium phosphate pH 8 containing 0.15 M NaCl and 100 mM imidazole. One fraction (the second 5 mL wash), which contained the majority of XPRTase-CHis, was desalted by passage through a Sephadex G-25 column bringing the enzyme into buffer A. The yields of the various protein forms were ≥50 mg per liter of bacterial culture.

Analysis of Nucleotide Content. Samples (200 μL) of XPRTase (in appropriate dilution) were mixed with 20 μL of a 1:1 mixture of concentrated perchloric and sulfuric acid. After 30 min of incubation at 0 °C the precipitated protein was removed by centrifugation at the maximal speed of a refrigerated Eppendorf centrifuge. The UV-absorption spectrum of the supernatant was recorded using a Specord S10 instrument from Zeiss. Samples of the buffer (200 μL) were treated similarly and used as references. The nucleotide content was also analyzed by denaturing the enzyme in 6 M GdHCl, subjecting it to gel filtration on a 10 mL Sephadex G-25 column (PD10) in buffer A containing 6 M GdHCl to separate macromolecules from the small molecules, and recording the UV-absorption spectra. The procedures have been described in detail previously (*27*).

Assays of XPRTase Activity. The conversion of xanthine to xanthosine generates large spectral changes due to a decrease of the pK_a value (from pH 7.7 to pH 5.7) of the purine base (*5*). Similar spectral changes resulted from the conversion of xanthine to XMP (not shown). By spectral analyses of the substrate (xanthine) and product (XMP) we found an isosbestic point at 252 nm where the change in absorbance from the conversion of xanthine to XMP (ΔA_{252} = 5.35 mM^{-1} cm^{-1}) was independent of pH. The standard assay for XPRTase was carried out at 25 °C by monitoring the absorbance at 252 nm as a function of time using the enzyme in an appropriate dilution. The reaction mixtures contained 50 mM Tris-HCl pH 7.6, 10 mM $MgCl_2$, 1 mM PRPP, and 50 μM xanthine. Reactions were started by addition of xanthine to a mixture of the other components (buffer, magnesium ions, enzyme, and PRPP) prewarmed at 25 °C for 5 min. One unit of enzyme activity is defined as the amount of enzyme that converts 1 μmol of xanthine to XMP under these standard conditions.

Substrate Specificity. To analyze the specificity for purine bases and the influence of potential allosteric effectors the enzyme was incubated under similar conditions using ^{14}C-labeled purine bases as substrates. Following preincubation (in a total volume of 40 μL) with all other components the ^{14}C-labeled purine base (10 μL) was added to initiate reaction. The time course of formation of the nucleotide product was monitored by extraction and subsequent application of 10 μL samples to polyimine impregnated cellulose thin layer plates at different times. The nucleotide product was separated from the base by chromatography in 0.9 M acidic acid containing 0.3 M LiCl, and the amount of product (and substrate) was quantified by use of an Instant Imager from Canberra-Packard.

Enzyme Kinetics and Analysis of pH Effects on the Reaction. The assays described above were employed with other concentrations of substrates and other buffers. The concentrations employed are given in the text where appropriate.

Ligand Binding Assays. The radioactively labeled ligands (0.2−2 TBq mol^{-1}) were incubated for 10 min with XPRTase (ca. 25 μM) at room temperature in a buffer consisting of 50 mM Tris-HCl pH 7.6 and 10 mM $MgCl_2$. The total volume was 200 μL. Samples (20 μL) were collected and counted to determine the total concentration of ligand. Other samples (150 μL) were applied to Ultrafree-MC spin devices (Amicon) and centrifuged at 5000*g*. The radioactivity in 20 μL aliquots of the liquid that had passed through the molecular filter was counted to determine the concentration of free (unbound) ligand (*27*). The concentrations of total and free PRPP were determined by chromatography using poly(ethyleneimine)-impregnated cellulose thin-layer plates (*28*), since the preparation of [^{32}P]PRPP contained about 15% radioactive impurities, mostly orthophosphate.

Molecular Size Determination. The size of the native enzyme was determined by filtration through a Superose 12 column (size 25 mL) from Pharmacia using buffer A containing 10 mM $MgCl_2$ or buffer A containing 10 mM $MgCl_2$ and 1 mM PRPP. Yeast alcohol dehydrogenase (M_r = 150 000) and *E. coli* orotate phosphoribosyltransferase (M_r = 45 000) were used as markers of known size. Fractions (0.25 mL) were collected and analyzed for enzyme activities. The experiment was carried out using different concentrations of ligand free XPRTase. In the one set of runs the enzyme (100 μL) was applied to the column at a concentration of ca. 0.1 mg/mL. In other runs without PRPP the protein was applied to the column at concentrations of ca. 0.7 and 7 mg/mL.

Data Treatment. Ligand binding data were approximated to a hyperbolic binding behavior according to eq 1 using the Biosoft program Ultrafit,

$$[L_b] = (B_{max}[L_f])/(K_D + [L_f]) \quad (1)$$

in which $[L_b]$ is the concentration of bound ligand and $[L_f]$ the concentration of free ligand, K_D is the dissociation constant, and B_{max} is the maximal concentration of bound ligand at a given concentration of enzyme.

For determination of kinetic constants we used the Michaelis−Menten equation:

$$v = (V_{max}[S])/(K_M + [S]) \quad (2)$$

Kinetic data relating to product inhibition were analyzed by use of the equation for competitive inhibition,

$$v = (V_{max}[S])/(K_{M,A}(1 + [I]/K_I) + [S]) \quad (3)$$

or the equation applying to noncompetitive (also called mixed-type) inhibition,

$$v = (V_{max}[S])/(K_{M,A}(1 + [I]/K_{IS}) + [S](1 + [I]/K_{II})) \quad (4)$$

The K_M for xanthine was also determined from reactions in which the enzyme had been preincubated with PRPP (2 mM) and mixed with an equal volume of xanthine (10 or 20 μM) at time $t = 0$ in a stopped flow apparatus (SX-18MW) from Applied Photophysics. The increase of light absorbance at 252 nm (A_{252}) was monitored as function of time until all xanthine was converted to XMP. The kinetic parameters were then determined by using the integrated Michaelis−Menten equation (*29*) in the form

$$[P]_t = V_{max}t - K_M\ln([S]_{t=0}/[S]_t) \quad (5)$$

The curvature of the accelerating reactions could be analyzed by the equation describing the behavior of hysteretic enzymes (*30*):

$$[P]_t = V_{ss}t - (V_{ss} - V_{ini})(1/k)(1 - e^{-kt}) \quad (6)$$

In eqs 5 and 6, $[S]_t$ is the concentration of remaining substrate at given time t, $[P]_t$ = the concentration of product at time t, V_{ini} is the initial reaction rate just after start, V_{ss} is the steady-state rate that the reaction approaches, and k is the rate constant for the transition of the enzyme from a low activity form (or an inactive form) to a more active form.

Crystallization. Prior to crystallization the XPRTase−GMP complex prepared as described above was dialyzed against buffer A containing 10% glycerol and kept at 4 °C. Crystallization of the protein was carried out by vapor diffusion in hanging drops kept at room temperature. Crystal Screen I from Hampton Research (*31*) was used for initial screening of crystallization conditions. The hanging drops were equilibrated over a 1 mL reservoir solution containing 10% glycerol, which was added after mixing the drop, to compensate for the glycerol in the protein solution. The crystal used for data collection was grown at room temperature from a drop made of 2 μL of 3.6 mg/mL XPRTase in complex with GMP, mixed with 2 μL of reservoir solution. The reservoir solution contained 25% (w/v) poly(ethylene glycol) 8000, 150 mM calcium chloride, 100 mM sodium acetate, and 100 mM morpholine ethanesulfonic acid pH 6.5. At these conditions, crystals appear within a couple of days.

Data Collection and Processing. The XPRTase crystals could be frozen directly in liquid nitrogen as the mother liquor acts as cryoprotectant. An X-ray diffraction data set (I) extending to 2.5 Å resolution was collected on a crystal cooled to 120 K using a MAR-research 345 imaging plate device mounted on a copper rotating anode generator from Rigaku (RU300) operating at 50 kV/80 mA. An additional data set (II) was collected from the same crystal cooled to 100 K at beam line X11 at the DESY outstation (EMBL, Hamburg, Germany) equipped with a MAR research 165 CCD detector and with synchrotron radiation the diffraction data extended to 2.05 Å resolution. Autoindexing, data reduction, and scaling were performed with programs from the HKL suite (*32*). The structure factors were derived from the reflection intensities using TRUNCATE (*33*). Statistics for the diffraction data collections are shown in Table 1. Analysis of the diffraction pattern showed that the crystal belongs to the orthorhombic space group $P2_12_12_1$. Cell dimensions and details about the data collection and reduction are given in Table 1.

Table 1: Data Collection and Refinement Statistics

enzyme	wild type	wild type
ligands	GMP	GMP
Crystal Parameters		
space group	$P2_12_12_1$	$P2_12_12_1$
a (Å)	53.5	53.6
b (Å)	54.3	54.3
c (Å)	138.6	138.8
no. of subunits per asu	2	2
Data Collection Statistics		
resolution range (Å)[a]	25−2.5 (2.59−2.50)	20−2.05 (2.12−2.05)
no. of observations	114503	92585
no. of unique reflections	14519	22917
mosaicity (deg)	1.1	1.0
R_{merge}[a]	0.088 (0.466)	0.073 (0.369)
completeness[a]	0.995 (0.976)	0.893 (0.914)
$I/\sigma(I)$[a]	21.2 (3.21)	16.7 (3.02)
Refinement Statistics		
resolution range (Å)[a]		20−2.05 (2.12−2.05)
no. of reflections used in *R*		21789
no. of reflections used in R_{free}		1128
R[a]		0.211 (0.271)
R_{free}[a]		0.252 (0.293)
rmsd for bond lengths (Å)		0.006
rmsd for bond angles (deg)		1.3
Ramachandran plot (% allowed, generously allowed, and disallowed residues)		98.8, 1.2, 0.0
no. of atoms (protein, ligands, water)		2890, 54, 144
av *B*-factors (Å^2 protein, ligands, waters)		38.0, 33.8, 37.8

[a] The numbers in parentheses refer to the outermost resolution shell.

Structure Determination. The structure could be determined by the molecular replacement (MR) despite the low sequence identity (22%) to the applied search model, a subunit of APRTase from *Giardia lamblia* (Protein Data Bank accession code 1L1R) (*34*). The search model had all its residues substituted with alanines except for glycines. The program AMoRe (*35*) was used for molecular replacement search with reflections from data set I in the range 15−4.5 Å. The self-rotation function, calculated using data set I, in the resolution range 5−2.5 Å, revealed a 2-fold axis perpendicular to the crystallographic *c*-axis at an angle = 38.5° to the *a*-axis. This observation is consistent with the assumption of two protein chains per asymmetric unit with a corresponding solvent content of 49% (*36*). The rotation search utilizing the locked rotation function gave two solutions with significantly higher correlation coefficient than the remaining solutions. The translational searches were performed using the centered correlation function of AMoRe (*37*). Number three of the first one-body translational search led to the correct solution, characterized by a clear contrast in the values of the correlation coefficients compared to incorrect solutions when both subunits were placed. The correlation coefficient for the final solution was 35.8% after rigid body refinement. Mutations and manual rebuilding were done in the graphic display program O (*38*). This initial model with an *R*-factor of 0.42 (R_{free} = 0.49) was used as

input to the program ARP/wARP (*39*). New electron density maps were calculated using the automatically rebuilt model obtained by ARP/wARP, and the remaining parts of the structure were easily built manually. The final refinement of the structure was carried out with CNS (*40*) using data set II and employing the automatic procedure for water insertion. The electron density in the $2F_o - F_c$ maps showed that the peptide bond Glu58−Ser59 adopts a *cis*-conformation. Restrained NCS symmetry was imposed between the two subunits in the dimer. The quality of the two monomers in the asymmetric unit was examined by using PROCHECK (*41*), which showed that no residues were in the disallowed regions of the Ramachandran plot. Further details on the structure refinement are listed in Table 1. The coordinates of the structure have been deposited in the Protein Data Bank (2FXV). A search in the PDB revealed a deposition of the coordinates of the *B. subtilis* XPRTase in complex with a GDP analogue (1Y0B) with diphosphate in the 3′ position without a supporting publication. The structural results derived from the coordinates of 1Y0B (*42*) support those described in the following.

Structure Analysis. The Protein-Protein Interaction Server (http://www.biochem.ucl.ac.uk/bsm/PP/server) was used for analysis of the dimer interface. Structure and sequence alignment was performed using the INDONESIA program package (http://xray.bmc.uu.se/∼dennis).

RESULTS

Purification and Formation of Nucleotide Free, GMP and XMP Saturated Complexes. In initial experiments the XPRTase seemed unable to use guanine or hypoxanthine as substrates. We were therefore surprised to find that the histidine-tagged enzyme, purified by chromatography on a Ni-chelate column, released substantial amounts of a guanine nucleotide (GMP) following denaturation with acid or treatment with 6 M guanidinium chloride (Figure 3A,B). The native, untagged enzyme also contained the nucleotide, but most of it could be removed by repeated precipitation with 80% ammonium sulfate and DEAE cellulose chromatography. We observed that the nucleotide free enzyme adsorbed to the Dyematrex Gel Red A column material, while the enzyme−nucleotide complex did not bind. Hence, a nucleotide free enzyme could be prepared by chromatography on a column of Dyematrex Gel Red A column, eluting the bound material with sodium chloride, while XPRTase−XMP and XPRTase−GMP complexes were obtained by eluting the enzyme with buffers containing 1 mM XMP or GMP, respectively. Absorption spectra of the three enzyme forms are shown in Figure 3. The absorbance of the apo-enzyme is very low ($A_{280} = 2560$ M^{-1} cm^{-1} (*43*)) due to the content of only two tyrosines (and no tryptophans) in the protein. Hence most of the UV absorbance of the complexes stems from the bound nucleotide.

Oligomeric State and Reaction Start. The oligomeric state of XPRTase was determined by size exclusion chromatography as described in Materials and Methods. When concentrated enzyme solutions were applied to the column, the ligand free protein migrated as a dimer (42 kDa). In more dilute solution, XPRTase migrated as a 42 kDa protein in the presence of PRPP (1 mM), but appeared smaller (32 kDa depending on protein concentration) in the absence of PRPP,

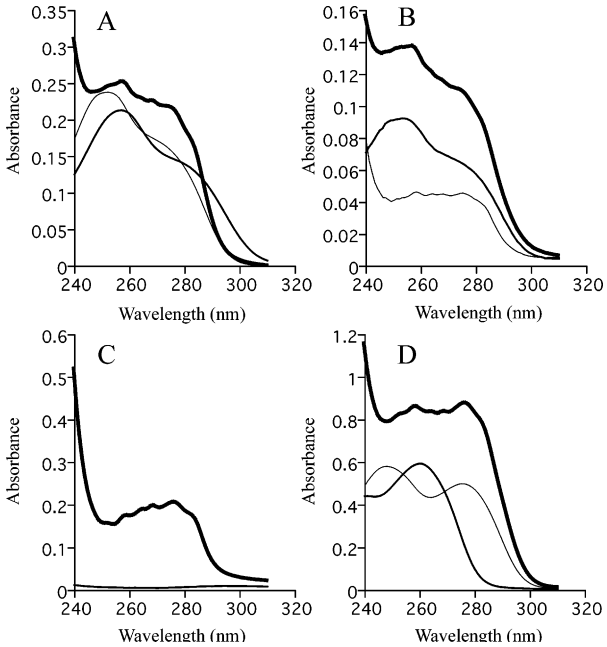

FIGURE 3: UV-absorption spectra of various XPRTase−nucleotide complexes. (A) Spectrum of His_6-tagged XPRTase purified by Ni^{2+} column chromatography. Thick line: the native protein. Middle thick line: acid supernatant after removal of the precipitated protein by centrifugation. Thin line: calculated spectrum at neutral pH assuming that the absorbance stems from GMP. (B) Spectra of His_6-tagged XPRTase, purified by Ni^{2+} column chromatography, unfolded in 6 M GdHCl and subjected to chromatography on a PD10 column. Thick line: the enzyme before chromatography. Middle thick line: spectrum of low MW substances after chromatography in 6 M GdHCl. Thin line: the macromolecules after chromatography in 6 M GdHCl. (C) Thick line: spectrum of nucleotide free enzyme. Thinner line: spectrum of acid supernatant. (D) Enzyme−XMP complex. Thick line: spectrum of native enzyme complex. Middle thick line: spectrum of acid supernatant. Thin line: calculated absorption spectrum of XMP at neutral pH. The spectra of the prepared (untagged) XPRTase−GMP complex were very similar to the spectra in panel A and are therefore not shown.

indicating a tendency of the ligand free enzyme to dissociate into monomers. Reactions initiated by addition of xanthine to mixtures containing enzyme and PRPP proceeded at a constant rate (V_{ss}) from the start. In contrast, when the reactions were initiated by addition of PRPP to mixtures containing enzyme and xanthine, they exhibited an accelerating phase with an initial reaction rate (V_{ii}) close to zero, which gradually approached the steady state rate V_{ss} (Figure 4A). The rate constant (termed "*k*" in eq 6) describing the transition from inactive to active (dimeric) enzyme was proportional with the protein concentration (data not shown). This is in accordance with the notion that the assembly of inactive monomers to dimers is responsible for the activation, rather than a time-consuming conformational change. The active dimeric form of XPRTase was also stabilized by XMP or GMP, since the reactions started with PRPP also proceeded as linear functions of time when these nucleotides (at 40 μM) were included in the preincubation mixtures together with the enzyme. PP_i (1 mM) had some stabilizing influence, but did not fully promote steady state kinetics from the start.

Effects of pH on Specificity for Purine Bases. The specificity for the purine bases was first investigated at pH 8.8. An experiment in which the enzyme was allowed to

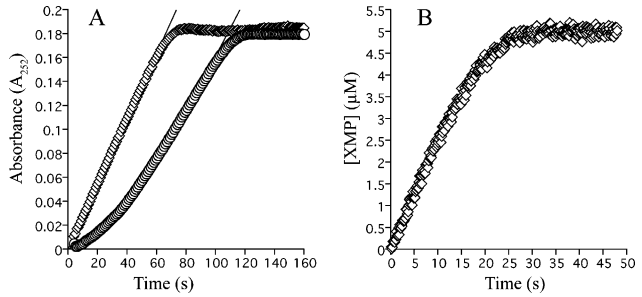

FIGURE 4: Progress curves for the conversion of xanthine and PRPP to XMP as catalyzed by XPRTase. (A) This panel shows that the initial reaction kinetics depends on order of assembly of the assay mixtures. (◇) Enzyme was preincubated (3 min) with 1 mM PRPP prior to initiation of reaction by addition of xanthine (40 μM). (○) Enzyme was preincubated (3 min) with xanthine prior to start of reaction by addition of 1 mM PRPP. The initial phases of two reactions were analyzed using eq 6 (*30*) describing the behavior of hysteretic enzymes. When the enzyme was preincubated with PRPP and started with xanthine, the initial velocity (V_{ini} = 0.0024 ± 0.0008ΔA_{252} s^{-1}) was equal to the steady state rate (V_{ss} = 0.002725 ± 0.000007ΔA_{252} s^{-1}). When the enzyme was preincubated with xanthine and started with PRPP, the initial velocity was V_{ini} = 0.00031 ± 0.00002ΔA_{252} s^{-1} and the steady state rate was V_{ss} = 0.00298 ± 0.00007ΔA_{252} s^{-1}. The apparent rate constant for conversion of the (inactive) enzyme to an active form was k = 0.020 ± 0.001 s^{-1}. (B) This panel shows the progress of a reaction when the enzyme was allowed to convert 5 μM xanthine to XMP in the presence of 1 mM PRPP and after preincubation with 2 mM PRPP. Analysis using the integrated Michaelis−Menten equation (eq 5) revealed an apparent $K_{M,xanthine}$ = 2.2 ± 0.1 μM (at 1 mM PRPP) and k_{cat} = 11 s^{-1}.

exhaust a limited supply of xanthine in the presence of 1 mM PRPP (Figure 4B) revealed a turnover number k_{cat} = 11 s^{-1} and a $K_{M,xanthine}$ = 2.2 ± 0.1 μM ($k_{cat}/K_{M,xanthine}$ = 5 × 10^6 M^{-1} s^{-1}), and steady state velocity measurements at 50 μM xanthine showed $K_{M,PRPP}$ = 30 ± 3 μM. No activity was detected with adenine as substrate, but the enzyme could use guanine and hypoxanthine as poor substrates with k_{cat}/K_M values approximately 10^{-4} times the corresponding values for xanthine. With guanine the parameters were k_{cat} = 0.03 s^{-1} and $K_{M,guanine}$ = 281 ± 32 μM (at 1 mM PRPP). With hypoxanthine they were k_{cat} = 0.5 s^{-1} and $K_{M,hypoxanthine}$ = 1250 ± 150 μM (at 1 mM PRPP).

Figure 5 shows how the activities with xanthine and hypoxanthine vary as a function of pH. The activity profiles for both substrates can be explained as corresponding to the titration of two functional groups in the enzyme/substrate complex. The pK_a values for the rising phase toward increasing pH were 7.4 ± 0.1 for xanthine and 8.6 ± 0.2 for hypoxanthine, while the pK_a for the declining phase at high pH values was 10.3 for both purine bases. The K_M for both bases remained almost constant in the pH interval 6 to 9, while the catalytic rate (k_{cat}) increased. Above pH 9 the k_{cat} declined while K_M increased for both bases. Activity with guanine was extremely low at pH below 8. It increased at more alkaline pH, but no detailed investigation of the pH−activity profile was made.

Product Inhibition. The inhibition by products was investigated with PRPP as the variable substrate keeping xanthine at a fixed concentration (40 μM). The inhibition by XMP was strictly competitive against PRPP ($K_{IS,XMP}$ = 22 ± 3 μM) with the uncompetitive part being insignificant ($K_{II,XMP}$ > 10^{20} M). GMP also generated competitive inhibition against PRPP ($K_{IS,GMP}$ = 33 ± 9 μM and $K_{II,GMP}$ > 10^{17} M).

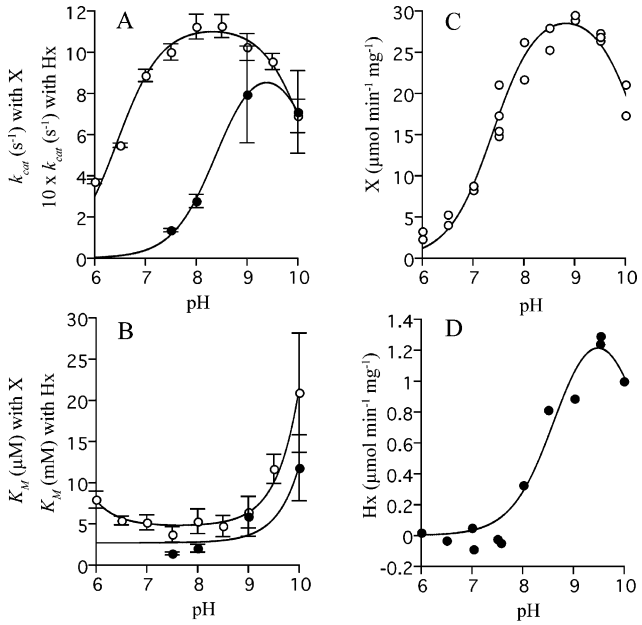

FIGURE 5: pH−activity profiles with xanthine (○) and hypoxanthine (●) as substrates. The reactions contained 1.2 mM PRPP, 10 mM $MgCl_2$, and buffers with different pH. (A) This panel shows the variation of k_{cat} as a function of pH. For hypoxanthine, the k_{cat} values were multiplied by a factor of 10 for the sake of clarity. (B) This panel shows variation of K_M as a function of pH. Note the different units, mM for hypoxanthine and μM for xanthine. (C) The specific activity as a function of pH assayed with xanthine (40 μM) as substrate. (D) The specific activity as a function of pH assayed with hypoxanthine (2.3 mM) as substrate. K_M and k_{cat} were determined from the initial velocities observed at 5 different concentrations of the purine base at two different concentrations (0.6 and 1.2 mM) PRPP, which gave same results. The graphs in panels A, C, and D were calculated from the data points by the least-squares method according to the equation parameter = $P/(1 + (10^{pK_a - pH}) + (10^{pH - pK_b}))$. For panel B the equation $K_M = K_M^{\#}(1 + (10^{pK_a - pH}) + (10^{pH - pK_b}))$ was used (*44*). For the specific activities with xanthine the parameters were pK_a = 7.4 ± 0.1, pK_b = 10.3 ± 0.1. For hypoxanthine they were pK_a = 8.7 ± 0.2 and pK_b = 10.3 ± 0.3. The parameters describing the variation of k_{cat} as a function of pH were pK_a = 6.5 ± 0.1 and pK_b = 10.2 ± 0.1 for xanthine, while they were pK_a = 8.4 ± 0.1 and pK_b = 10.4 ± 0.1 for hypoxanthine. The parameters describing the variation of K_M as a function of pH were pK_a = 5.8 ± 0.2 and pK_b = 9.4 ± 0.1 for xanthine. For hypoxanthine, pK_b = 9.5 ± 0.3, while no pK_a value could be determined.

The inhibition with pyrophosphate appeared noncompetitive. The competitive part was predominant ($K_{IS,PPi}$ = 580 ± 120 μM) while the uncompetitive part was weak ($K_{II,PPi}$ = 6800 ± 5500 μM). Attempts to determine product inhibition patterns at constant concentrations of PRPP and variable concentrations of xanthine failed because of the low K_M value for xanthine. None of the ribonucleoside triphosphates (ATP, GTP, CTP, and UTP) present at 1 mM concentration influenced the activity of the enzyme.

Ligand Binding. Ligand binding parameters were determined by a centrifugation technique described in Materials and Methods. Binding curves are shown in Figure 6. The dissociation constants were as follows: $K_{D,PRPP}$ = 2.2 ± 0.2 μM, $K_{D,XMP}$ = 2.1 ± 0.2 μM and $K_{D,GMP}$ = 4.5 ± 1.1 μM. The presence of PRPP inhibited binding of GMP and XMP (K_i = 2.2 ± 0.5 μM). XMP inhibited binding of GMP (and vice versa) with inhibition constants similar to the dissociation constants described above. [^{14}C]IMP binding takes place with a dissociation constant K_D = 19 ± 3 μM with the same

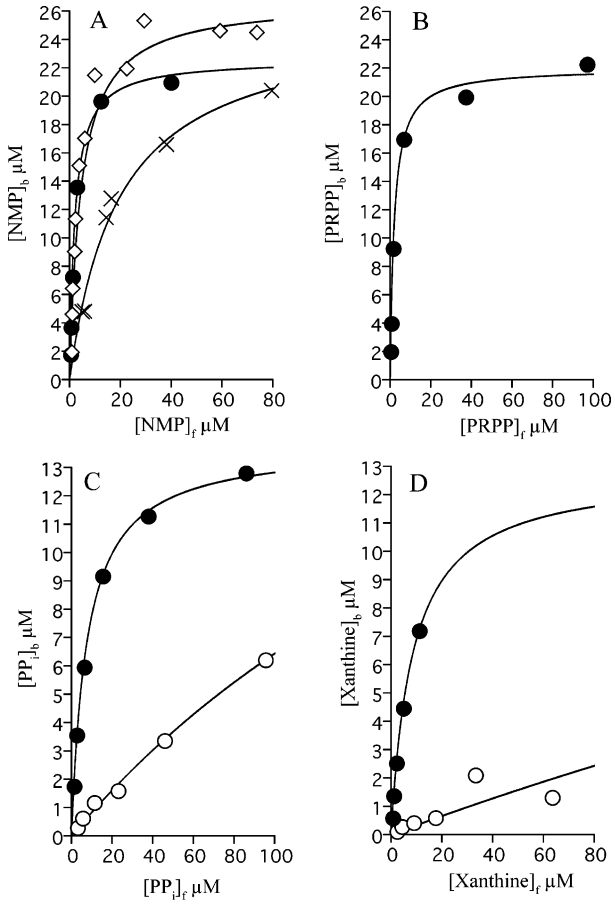

FIGURE 6: Binding of ligands. (A) XMP (●) $K_D = 2.1 \pm 0.2$ μM and $B_{max} = 22.6 \pm 0.7$ μM); GMP (◇) $K_D = 4.5 \pm 1.1$ μM and $B_{max} = 27 \pm 2$ μM; IMP (×) $K_D = 19 \pm 3$ μM and $B_{max} = 25 \pm 2$ μM. (B) PRPP $K_D = 2.0 \pm 0.2$ μM, $B_{max} = 22.0 \pm 0.5$ μM. (C) PP_i in the presence of 100 μM xanthine (●) $K_D = 7.8 \pm 0.4$ μM and $B_{max} = 13.8 \pm 0.2$ μM. PP_i alone (○) $K_D = 130 \pm 8$ μM, when B_{max} was set to 13.8 μM. (D) Xanthine in the presence of 1 mM PP_i (●) $K_D = 8.7 \pm 1$ μM and $B_{max} = 12.8 \pm 0.9$ μM. Xanthine alone (○) $K_D = 744 \pm 205$ μM. In the latter case B_{max} was set to 25 μM, since saturation was far from achieved and since twice as much enzyme was used for this experiment as for when the binding was assessed in the presence of 1 mM PP_i. The high concentration of protein used in the ligand binding assays means that the enzyme predominantly exists in the dimeric form in all cases.

number of binding sites as seen for GMP and XMP. Xanthine and pyrophosphate both bound poorly to the enzyme; therefore saturation could not be reached and the K_D values ($K_{D,xanthine} = 740 \pm 210$ μM and $K_{D,PPi} = 130 \pm 8$ μM) were calculated assuming the same number of binding sites for these ligands as observed for the nucleotides. However, xanthine and PP_i bound well when combined: $K_{D,xanthine} = 8.7 \pm 1.0$ μM in the presence of 1 mM PP_i and $K_{D,PPi} = 7.8 \pm 0.4$ μM in the presence of 100 μM xanthine (Figure 6B,C).

Crystal Structure. The crystal structure of the XPRTase−GMP complex was determined to 2.05 Å resolution by the molecular replacement (MR) method using the subunit of *G. lamblia* APRTase as search model. This successful application of the molecular replacement method is noteworthy due to the low sequence identify (22%) between *B. subtilis* XPRTase and *G. lamblia* APRTase. The structure of the dimeric XPRTase−GMP complex was refined to an *R*-factor of 0.21 ($R_{free} = 0.25$). It shows good geometry with more than 98% of the residues in the allowed regions of the Ramachandran plot and no residues in the disallowed regions. The statistics of the refinement are summarized in Table 1. The asymmetric unit of the XPRTase−GMP complex contains two subunits arranged as a homodimer with the subunits related by a 2-fold noncrystallographic axis (Figure 7B) in agreement with the oligomeric state of active XPRTase in solution. There is clear electron density for all amino acid residues in the model except for the last four C-terminal residues in both subunits (A 191−194, B 191−194), which it was not possible to localize in the electron density map.

Overall Fold. Each subunit comprises a compact single domain structure with a type 1 PRTase fold, which contains two subdomains: the core and the hood (Figure 7A). The hood subdomain is formed by N-terminal residues and comprises two β-strands and one α-helix. The electron density corresponding to the flexible loop, which contributes to the formation of the active site of the PRTases (*15*, *47*), is well-defined except for the residues 83−90. In the XPRTase−GMP complex it is closed over the active site. Residues located in β3, β4, β6, α2, α3, and γ1 contribute to the dimer formation; with 64% of the atoms in the interface between the two subunits being nonpolar, hydrophobic interactions must play a role in the stabilization of the dimer. The formation of the dimer buries 13% of the total accessible surface area of each subunit corresponding to a surface area of 1200 Å^2. The intersubunit interactions between the two subunits in the dimer include two salt bridges, fourteen neutral hydrogen bonds, and nine bridging waters. The separation between the active sites in the dimer is approximately 38 Å, measured as the distance between Nζ of Lys156 in the two subunits.

Binding of GMP. The binding site for purine base is defined by the position of the guanine moiety of GMP, which is bound in a cleft between the hood and the core. A detailed picture of the protein−GMP interactions is presented in Figure 7C and Figure 8. The guanine ring participates in hydrophobic interactions with the side chains of Thr100 and Phe99 from the flexible loop and Phe126 and Ala128 from the core. In addition the guanine ring is engaged in hydrogen bonds with three residues in the active site. The backbone carbonyl and amide group of Leu20 from the hood subdomain form hydrogen bonds to N1 and to the exocyclic O6 of the guanine moiety (Figures 7C and 8). Another hydrogen bond is formed between the side chain Oδ1 of Asn27 from the hood domain and the exocyclic N2-amino group of the guanine moiety. Lys156 is positioned at the end of the fourth β-strand in the central β-sheet (β8). The short distance between its ε-amino group and N7 of the guanine ring (2.67 Å) shows that the ammonium group of the side chain of Lys156 acts as a hydrogen bond donor to N7, suggesting that N7 is unprotonated. This is further supported by the absence of basic functional groups (carboxylates) in the neighborhood of N7 that could stabilize a protonated form of N7.

DISCUSSION

Reaction Mechanism. The very weak binding of xanthine to the free enzyme ($K_D \approx 740$ μM) relative to the strong binding of PRPP ($K_D \approx 2$ μM) shows that the mechanism for all practical purposes is ordered with PRPP binding first and the nucleotide being the last product to dissociate from

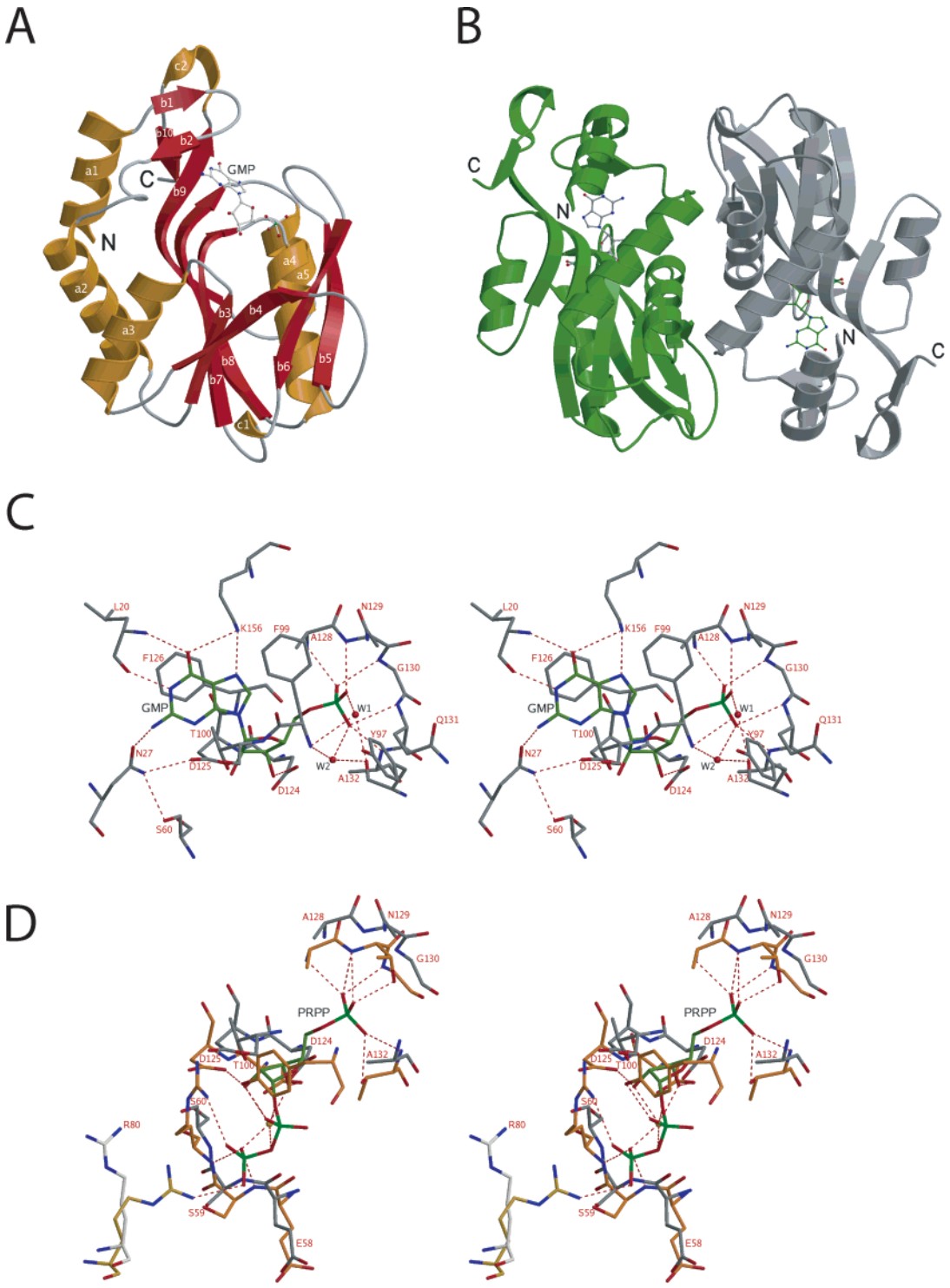

FIGURE 7: Crystal structure of XPRTase. Each subunit comprises a compact single domain structure composed of 10 β-strands (β1−β10), five α-helices (α1−α5), and two 3_{10}-helices (γ1−γ2), which can be attributed into two subdomains: the core and the hood. As in all type 1 PRTases, the core subdomain consists of a central five-stranded parallel β-sheet (β4, 76−82; β3, 53−57; β7, 119−127; β8, 146−156; β9, 172−188) sandwiched between α-helices (α2, 31−46; α3, 61−73; α4, 130−143; α5, 160−167) (*55*). The hood subdomain is formed by N-terminal residues and comprises two β-strands and one α-helix (β1, 13−14; β2, 20−21; α1, 1−12). The segment consisting of residues 83−111, including β5 (91−97) and β6 (104−110), forms the so-called flexible loop. Ribbon views of the subunit (A) and the homodimer (B) of XPRTase from *B. subtilis*. GMP is shown in ball-and-stick representation. (C) Stereoview of the GMP binding in XPRTase. (D) Stereoview of the PRPP binding (green). Residues from APRTase are displayed in orange, while residues from XPRTase are displayed in gray. Residues shown in lighter colors are from the adjacent subunit. The numbering is according to *B. subtilis* XPRTase. Hydrogen bonds are represented with red broken lines. The illustrations were prepared using MOLSCRIPT (*45*) and RASTER 3D (*46*).

the enzyme. These compounds are the same that promote assembly of the protein from an inactive monomer to an active dimer. Under extreme conditions the enzyme may use the alternative path of substrate addition, but the two "arms" of the potentially random mechanism (Figure 9) are not in thermodynamic equilibrium, since an equilibrium situation would require that $K_{D,PRPP}$ (2 μM) × $K_{M,xanthine}$ (2−3 μM) equals $K_{D,xanthine}$ (740 μM) × $K_{M,PRPP}$ (30 μM), which

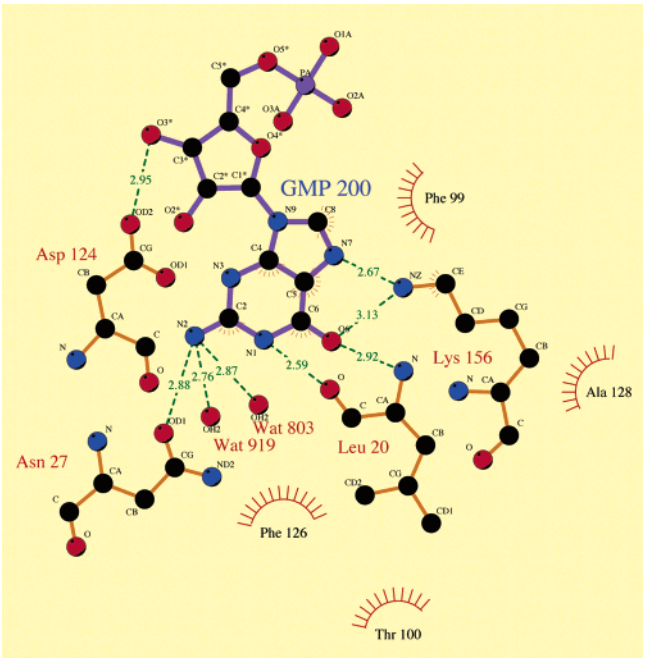

FIGURE 8: LIGPLOT (*48*) diagram of the hydrogen bonding pattern, and hydrophobic interactions with GMP bound in subunit B of XPRTase. Explanation: Blue lines, ligand bonds; orange lines, nonligand bonds; broken green lines, hydrogen bonds and their lengths; "eyelashes", enzyme residues and corresponding ligand atoms involved in hydrophobic interactions.

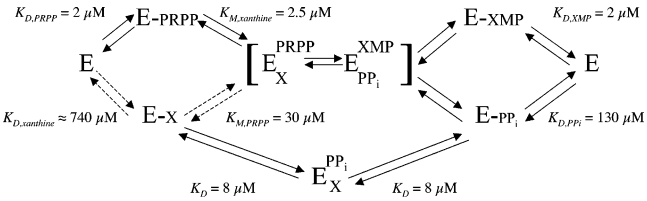

FIGURE 9: Hypothetical random reaction mechanism in accordance with initial velocity kinetics, product inhibition patterns, and ligand binding analyses. The indicated K_D values summarize the results of the ligand binding analyses, and the K_M values were from initial velocity measurements. The very weak binding of xanthine as well as thermodynamic arguments (see text) argue against a random mechanism, indicating that the mechanism for all practical purposes is ordered with PRPP binding first. Products may still be released in a random fashion.

obviously is not the case (Figure 9). The competitive inhibition by XMP against PRPP and the noncompetitive inhibition produced by PP_i are in agreement with both mechanisms due to the occurrence of the relatively strong E−PP_i−xanthine complex. An analysis of the initial velocity kinetics of the XPRTase from *E. faecalis* published in 1974 (*12*) indicated that that enzyme employed a ping-pong mechanism. However, during the recent years, several publications have illustrated how special features of individual PRTases may lead to initial velocity kinetics similar to that of ping-pong reactions (*27*, *49*, *50*) although more detailed analyses revealed that they all used sequential mechanisms.

Substrate Specificity and Nucleotide Binding. The extreme selectivity of *B. subtilis* XPRTase for xanthine is remarkable and is only matched by the specificity of the XPRTase from *E. faecalis* (*12*), whose structure is unknown. Our initial studies indicated that the enzyme only used xanthine as the purine base substrate, but when it turned out that the enzyme expressed in *E. coli* contained substantial amounts of GMP, we investigated the activity with the purine bases in greater detail. Our investigations revealed that though the activity with hypoxanthine and guanine increased at more alkaline pH, at optimal pH the catalytic efficiency (k_{cat}/K_M) with xanthine was still approximately 10^4 times higher than with guanine or hypoxanthine.

The pH−activity profiles with xanthine and hypoxanthine differed from each other, but both could be explained by the titration of two protons. In the pH interval $6 \leq pH \leq 9$ the turnover number k_{cat} increased with pH, while K_M was unaffected. The pK_a values, describing the increase in activity as a function of pH (i.e. pK_a = 7.4 ± 0.1 for xanthine and 8.6 ± 0.2 for hypoxanthine), correspond to the acidity constants of the purine bases in solution (pK_a = 7.7 for xanthine (*5*) and pK_a = 8.9 for hypoxanthine (*51*)). Thus, it appears that the negative charge, which develops on the purine base with increasing pH, is a requirement for catalysis (passing of the transition state), but not for binding of the purine in the Michaelis complex. The crystal structure provides further evidence for this interpretation. It reveals that the *B. subtilis* XPRTase lacks a catalytic base (a glutamate or an aspartate) in the active site, near N7 of the purine base as found in all characterized enzymes belonging to the major class of 6-oxo purine PRTases. In the human HGPRTase, which prefers the neutral form of the purine base and excludes xanthine as a substrate, the carboxylate group of Asp137 has been ascribed the function of stabilizing the N7-protonated tautomer of the purine, thereby releasing the lone pair on N9 for glycosyl bond formation (*52*). Since XPRTase lacks a similarly positioned carboxylate group, the successful catalysis depends on the ability of the purine base to deprotonate spontaneously.

In more alkaline solution (pH > 9) the K_M values for xanthine and hypoxanthine increase with rising pH while the k_{cat} for both bases decreases with a pK_a close to 10.3. This value of pK_a indicates that a positive charge on a lysine residue in the enzyme is important for both catalysis and substrate binding in the ground state. The crystal structure suggests that this critical lysine is Lys156, which is within hydrogen bond distance (2.67 Å) from N7 of the bound nucleotide, GMP (Figures 7C and 8). Furthermore a similarly positioned lysine is found in all 6-oxo purine PRTases. It was ascribed two functions in the human HGPRTase as it acts as a proton donor during pyrophosphorolysis of nucleotides (i.e. nucleotide cleavage) and also as a contributor to the binding of purine bases (*52*). Our results support that the positive charge on Lys156 contributes to the binding of the negatively charged purine base in the Michaelis complex of XPRTase; however, its role in catalysis (k_{cat}) is not so transparent.

The ability of the active site to bind both XMP (K_D = 2 μM) and GMP (K_D = 4 μM) with high affinity may be assigned to the asparagine residue (Asn27) located in the hood subdomain of XPRTase. The crystal structure shows that the amide group of Asn27 functions as proton acceptor in the hydrogen bond formed with the 2-amino group of GMP. With a simple rotation of 180° of the amide group it will be able to function as a proton donor in hydrogen bond formation with the 2-oxo group of XMP. IMP can also be accommodated in the binding site of XPRTase with a 5- to 10-fold lower affinity than XMP and GMP, which is

explained by the inability of this nucleotide to participate in hydrogen bonding at the 2-position. The fact that the enzyme when isolated from the cells contains GMP rather than XMP must be because the intracellular pool of GMP is much higher than the pools of XMP and IMP (P. Nygaard and K. F. Jensen, unpublished observations). In addition the strong binding of GMP may have a regulatory function so that XPRTase only is active under growth conditions causing shortage in the supply of guanine nucleotides and so that the cells catabolize xanthine (*14*) instead of converting it to nucleotide level, when the supply of guanine nucleotides is ample.

The enzyme's requirement for a negative charge on the purine base as a prerequisite to pass the transition state explains why xanthine ($pK_a = 7.7$) is a much better substrate than hypoxanthine ($pK_a = 8.9$) and guanine ($pK_a = 9.6$) at neutral pH. It is more difficult to explain the 10^4-fold preference for xanthine at pH around 9. In such solutions hypoxanthine is mainly negatively charged. The major discrimination against hypoxanthine relative to xanthine stems from an approximately 10^3-fold higher K_M for binding hypoxanthine (relative to xanthine) in the Michaelis complex, i.e., to the enzyme−PRPP complex. The crystal structure of the enzyme−GMP complex provides no mechanistic explanation of this large difference between the two bases in the affinity for binding in the ground state, although the lack of a hydrogen bond between Asn27 and the 2-position of the hypoxanthine moiety is expected to cause an increase in K_M. This bond contributed to the 10-fold higher affinity for XMP than for IMP. The difference in pK_a values for the two free bases reflects differences in the electron distribution in the purine ring system. The tighter binding of xanthine might suggest stronger electrostatic interactions between xanthine and the active site than is the case for hypoxanthine. The lack of the hydrogen bond could suggest further differences in the electron distribution in the transition state as the mechanism behind the 10-fold lower k_{cat} for hypoxanthine relative to xanthine. To substantiate this hypothesis for the difference in K_M and k_{cat} values would naturally require theoretical calculations of the electrostatic potential of the base and the active site.

Significant activity with guanine could only be detected at pH ≥ 8, and the kinetic parameters were only determined at pH 8.8 for that substrate. At this pH, the k_{cat} was only 0.03 s^{-1}, i.e. ≈15 times lower than with hypoxanthine and ≈300 times lower than with xanthine. Under these conditions, 16% of guanine ($pK_a = 9.6$) is expected to carry a negative charge. This will have an impact on the k_{cat} since a negative charge on the purine base seems to be a requirement for catalysis. It may also be relevant in this context that the proton dissociates from N1 of guanine at high pH, while it dissociates from N3 of xanthine (*5*). The ca. 5-fold lower K_M for guanine than for hypoxanthine could be explained by the ability of guanine to hydrogen bond with Asn27 in the enzyme. There are no obvious explanations for the approximately 100-fold lower affinity for guanine, relative to xanthine, but it is likely related to the different charge distributions within the two bases as described above for hypoxanthine. Interestingly, an unusually low catalytic rate constant (k_{cat}) for guanine relative to the other purine bases was also observed for the XPRTase from *L. donovanii* which has a high preference for xanthine, but according to sequence belongs to the major family of 6-oxo purine PRTases (Figure 2) (*10*).

The Family of Xanthine Phosphoribosyltransferases. Numerous sequences closely related to the *xpt* gene of *B. subtilis* are deposited in the sequence databases. Their occurrence is restricted to Gram-positive bacteria. These genes probably all encode similarly specific enzymes as the XPRTase from *B. subtilis*, but aside from this enzyme and the XPRTase from *E. faecalis* (*12*) none of them have been purified and characterized. According to their sequences, and the structure described herein, these enzymes belong to a very special subclass of the 6-oxo purine PRTases. They resemble the *B. subtilis* PurR repressor and a group of adenine PRTases (Figure 2) more than representatives of the major group of 6-oxo purine PRTases. Like the *B. subtilis* XPRTase, the PurR repressor and the APRTases are characterized by having a very small and simple hood domain interacting with the base moiety of bound nucleotides. They share this property with the orotate PRTases involved in pyrimidine nucleotide synthesis (*15*). So, what features of the enzyme determine the extreme preference for xanthine of this class of XPRTases? A most obvious factor is clearly the lack of a carboxylate group (from aspartate or glutamate) to stabilize the N7-protonated tautomer of the purine base and thus liberate N9 for glycosyl bond formation. This has the consequence that the Gram-positive XPRTases only can react with the negatively charged form of the purine base, and it gives itself a preference for xanthine, since this purine base is the most prone to dissociate a proton at neutral pH. Another feature is the deviant PRPP binding motif of the XPRTases, which contains two neighboring aspartate residues, while the major class of 6-oxo purine PRTases carry a PRPP binding motif that contains a glutamate residue followed by an aspartate. This second feature, however, is not unique to the XPRTases, since it is also found in the special class of XGPRTases, prevailing in *E. coli* and related bacteria, which react equally well with xanthine and guanine, but exclude hypoxanthine (Figure 2B). The third feature is the occurrence of the amide group of asparagine residue (Asn27), which can form a hydrogen bond with substituents at the 2-position of the xanthine and guanine moieties of both the free bases and their nucleotides. Other 6-oxo purine PRTases, e.g. HXGPRTase of *T. gondii* (*7*, *8*) and XGPRTase of *E. coli* (*9*), bind the 2-exocyclic groups of GMP and XMP by interaction with backbone carbonyl groups and water-mediated hydrogen bonds to a glutamate side chain.

Oligomeric State and Stabilization of the Active Dimer. The oligomeric state of XPRTase from *B. subtilis* is a dimer in its functional state. The binding of PRPP or the nucleotide products (or PP_i) stabilizes the dimeric form, and it dissociates into inactive monomers in dilute solution when the ligands are not present. A dimeric structure was also proposed for the closely related XPRTase from *E. faecalis* on the basis of a particle mass of 42 kDa (*12*). The dimeric structure of these enzymes is in marked contrast to the major class of 6-oxo purine PRTases, which form tetrameric structures (*4*, *6*). It is however striking that the proteins, which are the most related to XPRTase, i.e. the PurR repressor, the APRTases, and the OPRTases, also form active dimers.

To identify the interactions important for the dimer stabilization caused by the presence of PRPP, the structure

of XPRTase was superposed with the structure of *G. lamblia* APRTase in complex with PRPP. In the *G. lamblia* APRTase−PRPP complex the side chain Nη of Arg83 is positioned 2.9 Å from an α-phosphate oxygen of PRPP bound in the other subunit (*34*), and a similar interaction is observed in the *B. subtilis* PurR−cPRPP complex (*13*). This arginine residue is conserved between *G. lamblia* APRTase and *B. subtilis* XPRTase (Arg80) (Figure 7D), and formation of this direct hydrogen bond may explain why the binding of PRPP stabilizes the dimeric form of the enzyme. This is further confirmed by the unpublished structure of *B. subtilis* XPRTase in complex with guanosine 3′-diphosphate (PDB ID 1Y0B). In this complex the ribose ring is oriented differently, but the diphosphate moiety is in the same position as in the *G. lamblia* APRTase−PRPP complex making interactions with Arg80 from the other subunit. A similar stabilization of a higher oligomeric form is observed for uracil phosphoribosyltransferase from *T. gondii* upon PRPP binding (*53*). Furthermore, a key element in recognition of PRPP in type 1 PRTases is a non-proline *cis*-peptide bond between Glu58 and Ser59 (*54*, *55*). In the XPRTase−GMP complex this *cis*-peptide bond is present and apparently stabilized by the dimer formation, since the *cis*-peptide bond allows Oγ of Ser59 to form a hydrogen bond to carboxyl oxygen from the side chain of Glu58 from the other subunit. The missing stabilization of the *cis*-peptide bond could be the explanation of why the monomeric form of the enzyme is inactive.

Analyses of the initial reaction velocities showed that preincubation of XPRTase with GMP or XMP has the same stabilizing effect of the active dimer as PRPP binding. Although the structure of the XPRTase−GMP complex does not reveal any direct interactions between bound GMP and the other subunit which could explain the stabilizing effect, the binding of GMP probably diminishes the mobility of the flexible loop. Two of the oxygen atoms in the 5′-phosphate moiety of GMP form water-mediated hydrogen bonds to the backbone carbonyl of Tyr97 and the backbone nitrogen of Phe99. In addition, the purine ring of GMP is making hydrophobic interactions with Phe99 and Thr100. These residues, Tyr97, Phe99, and Thr100, are all part of the flexible loop covering the active site. That interactions with the 5′-phosphate moiety of GMP are important for stabilization of the flexible loop is supported by the fact that the flexible loop is in a more open conformation in *B. subtilis* XPRTase in complex with guanosine 3′-diphosphate. Though the residues in the flexible loop only contribute to a minor part of the interactions between the subunits with less than 2% of the buried surface area created by residues in the flexible loop, it is likely that a highly mobile loop would interrupt dimer formation.

ACKNOWLEDGMENT

We thank Lise Schack for help with the production and purification of the enzymes and Flemming Hansen and Dr. Pernille Harris for assistance during diffraction data collection. Dr. Hans Henrik Saxild is thanked for the gift of plasmid pSS9, Dr. Martin Willemoës for helpful discussions throughout the work, and Dr. Wuxian Shi for making the structure of the *G. lambia* APRTase available to us before publication. We are grateful for the beam time provided at EMBL/DESY Hamburg and for the Danish Natural Science Research Council contribution to Dansync.

REFERENCES

1. Jensen, K. F. (1983) Metabolism of 5-phosphoribosyl 1-pyrophosphate (PRPP) in *Escherichia coli* and *Salmonella typhimurium*, in *Metabolism of Nucleotides, Nucleosides and Nucleobases in Microorganisms* (Munch-Petersen, A., Ed.) pp 1−25, Academic Press, London.
2. Nygaard, P. (1983) Utilization of preformed purine bases and nucleosides, in *Metabolism of nucleotides, nucleosides, and nucleobases in microorganisms* (Munch-Petersen, A., Ed.) pp 27−93, Academic Press, London and New York.
3. Schramm, V. L., and Grubmeyer, C. T. (2004) Phosphoribosyltransferase mechanisms and roles in nucleic acid metabolism, in *Progress in Nucleic Acids Research and Molecular Biology* (Moldave, K., Ed.) pp 261−304, Elsevier, New York.
4. Shi, W., Li, C. M., Tyler, P. C., Furneaux, R. H., Grubmeyer, C., Schramm, V. L., and Almo, S. C. (1999) The 2.0 Å structure of human hypoxanthine-guanine phosphoribosyltransferase in complex with a transition-state analog inhibitor, *Nat. Struct. Biol. 6*, 588−593.
5. Stoychev, G., Kierdaszuk, B., and Shugar, D. (2002) Xanthosine and xanthine. Substrate properties with purine nucleoside phosphorylases, and relevance to other enzyme systems, *Eur. J. Biochem. 269*, 4048−4057.
6. Héroux, A., White, E. L., Ross, L. J., and Borhani, D. W. (1999) Crystal structures of the *Toxoplasma gondii* hypoxanthine-guanine phosphoribosyltransferase-GMP and -IMP complexes: Comparison of purine binding interactions with the XMP complex, *Biochemistry 38*, 14485−14494.
7. Héroux, A., White, E. L., Ross, L. J., Davis, R. L., and Borhani, D. W. (1999) Crystal structure of the *Toxoplasma gondii* hypoxanthine-guanine phosphoribosyltransferase with XMP, pyrophosphate, and two Mg^{2+} ions bound: Insight into the catalytic mechanism, *Biochemistry 38*, 14495−14506.
8. Héroux, A., White, E. L., Ross, L. J., Kuzin, A. P., and Borhani, D. W. (2000) Substrate deformation in a hypoxanthine-guanine phosphoribosyltransferase ternary complex: the structural basis for catalysis, *Structure 8*, 1309−1318.
9. Vos, S., Parry, R. J., Burns, M. R., de Jersey, J., and Martin, J. L. (1998) Structures of free and complexed forms of *Escherichia coli* xanthine-guanine phosphoribosyltransferase, *J. Mol. Biol. 282*, 875−889.
10. Jardim, A., Bergeson, S. E., Shih, S., Carter, N., Lucas, R. W., Merlin, G., Myler, P. J., Stuart, K., and Ullman, B. (1999) Xanthine phosphoribosyltransferase from *Leishmania donovani*. Molecular cloning, biochemical characterization, and genetic analysis, *J. Biol. Chem. 274*, 34403−34410.
11. Hendrickson, N., Allen, T., and Ullman, B. (1993) Molecular characterization of phosphoribosylpyrophosphate synthetase from *Leishmania donovani*, *Mol. Biochem. Parasitol. 59*, 15−28.
12. Miller, R. L., Adamczyk, D. L., Fyfe, J. A., and Elion, G. B. (1974) Xanthine phosphoribosyltransferase from *Streptococcus faecalis*. Properties and specificity, *Arch. Biochem. Biophys. 165*, 349−358.
13. Sinha, S. C., Krahn, J., Shin, B. S., Tomchick, D. R., Zalkin, H., and Smith, J. L. (2003) The purine repressor of *Bacillus subtilis*: a novel combination of domains adapted for transcriptional regulation, *J. Bacteriol. 185*, 4087−4098.
14. Christiansen, L. C., Schou, S., Nygaard, P., and Saxild, H. H. (1997) Xanthine metabolism in *Bacillus subtilis*: characterization of the xpt-pbuX operon and evidence for purine- and nitrogen-controlled expression of genes involved in xanthine salvage and catabolism, *J. Bacteriol. 179*, 2540−2550.
15. Scapin, G., Grubmeyer, C., and Sacchettini, J. C. (1994) Crystal structure of orotate phosphoribosyltransferase, *Biochemistry 33*, 1287−1294.
16. Hershey, H. V., and Taylor, M. W. (1986) Nucleotide sequence and deduced amino acid sequence of *Escherichia coli* adenine phosphoribosyltransferase and comparison with other analogous enzymes, *Gene 43*, 287−293.
17. Hove-Jensen, B., Harlow, K. V., King, C. J., and Switzer, R. L. (1986) Phosphoribosylpyrophosphate synthetase of *Escherichia coli*. Properties of the purified enzyme and primary structure of the *prs* gene, *J. Biol. Chem. 261*, 6765−6771.

18. Lundegaard, C., and Jensen, K. F. (1999) Kinetic mechanism of uracil phosphoribosyltransferase from *Escherichia coli* and catalytic importance of the conserved proline in the PRPP binding site, *Biochemistry 38*, 3327−3334.
19. Thompson, J. D., Higgins, D. G., and Gibson, T. J. (1994) CLUSTAL W: inproving the sensitivity of progressive multiple sequence alignment through weighting, positions-specific gap penalties and weight matrix choice, *Nucleic Acids Res. 22*, 4673−4680.
20. Felsenstein, J. (1989) PHYLIP (Phylogeny interference package, version 3.5c)—distributed by the author, *Cladistics 5*, 164−166.
21. Jensen, K. F., and Mygind, B. (1996) Different oligimeric states are involved in the allosteric behavior of uracil phosphoribosyltransferase from *Escherichia coli*, *Eur. J. Biochem. 240*, 637−645.
22. Poulsen, P., Jensen, K. F., Valentin-Hansen, P., Carlsson, P., and Lundberg, L. G. (1983) Nucleotide sequence of the *Escherichia coli pyrE* gene and of the DNA in front of the protein-coding region, *Eur. J. Biochem. 135*, 223−229.
23. Randerath, K., and Randerath, E. (1967) Thin-layer separation methods for nucleic acid derivatives, *Methods Enzymol. 12A*, 323−347.
24. Andersen, J. T., Poulsen, P., and Jensen, K. F. (1992) Attenuation in the *rph-pyrE* operon of *Escherichia coli* and processing of the dicistronic mRNA, *Eur. J. Biochem. 206*, 381−390.
25. Deuschle, U., Kammerer, W., Gentz, R., and Bujard, H. (1986) Promoters of *E. coli*. A hierarchy of in vivo strength indicates alternate structures, *EMBO J. 5*, 2987−2994.
26. Miller, J. H. (1972) *Experiments in molecular genetics*, Cold Spring Harbor Laboratory, Cold Spring Harbor, NY.
27. Jensen, K. F., Arent, S., Larsen, S., and Schack, L. (2005) Allosteric properties of the GTP activated and CTP inhibited uracil phosphoribosyltransferase from the thermo-acidophilic archaeon *Sulfolobus solfataricus*, *FEBS J. 272*, 1440−1453.
28. Jensen, K. F., Houlberg, U., and Nygaard, P. (1979) Thin-layer chromatographic methods to isolate ^{32}P-labeled 5-phosphoribosyl-α-1-pyrophosphate (PRPP): determination of cellular PRPP pools and assay of PRPP synthetase activity, *Anal. Biochem. 98*, 254−263.
29. Orsi, B. A., and Tipton, K. F. (1979) Kinetic analysis of progress curves, *Methods Enzymol. 63A*, 159−183.
30. Neet, K. E.; Ainslie Jr., G. R. (1980) Hysteretic Enzymes, *Methods Enzymol. 64*, 192−226.
31. Jancarik, J., and Kim, S. H. (1991) Sparse matrix sampling: a screening method for crystallization of proteins, *J. Appl. Crystallogr. 24*, 409−411.
32. Otwinowski, Z., and Minor, W. (1997) Processing of X-ray diffraction data collected in oscillation mode, *Methods Enzymol. 276A*, 307−326.
33. French, S., and Wilson, K. (1978) On the treatment of negative intensity observations, *Acta Crystallogr. A 34*, 517−525.
34. Shi, W., Sarver, A. E., Wang, C. C., Tanaka, K. S., Almo, S. C., and Schramm, V. L. (2002) Closed site complexes of adenine phosphoribosyltransferase from *Giardia lamblia* reveal a mechanism of ribosyl migration, *J. Biol. Chem. 277*, 39981−39988.
35. Navaza, J. (1994) AMORE: an automated package for molecular replacement, *Acta Crystallogr. A 50*, 157−163.
36. Matthews, B. W. (1968) Solvent content of protein crystals, *J. Mol. Biol. 33*, 491−497.
37. Navaza, J., and Vernoslova, E. (1995) On the fast translation functions for molecular replacement, *Acta Crystallogr. A 51*, 445−449.
38. Jones, T. A., Zou, J.-Y., Cowan, S. W., and Kjeldgaard, M. (1991) Improved methods for building protein models in electron density maps and the location of errors in these models, *Acta Crystallogr. A 47*, 110−119.
39. Perrakis, A., Morris, R., and Lamzin, V. S. (1999) Automated protein model building combined with iterative structure refinement, *Nat. Struct. Biol. 6*, 458−463.
40. Brünger, A. T., Adams, P. D., Glore, G. M., DeLano, W. L., Gros, P., Grosse-Kunstleve, R. W., Jiang, J. S., Kuszewski, J., Nilges, M., Pannu, N. S., Read, R. J., Rice, L. M., Simonson, T., and Warren, G. L. (1998) Crystallography & NMR system: A new software suite for macromolecular structure determination, *Acta Crystallogr. D 54*, 905−921.
41. Laskowski, R. A., MacArthur, M. W., Moss, D. S., and Thornton, J. M. (1993) PROCHECK: a program to check the stereochemical quality of protein structures, *J. Appl. Crystallogr. 26*, 283−291.
42. Cuff, M. E., Wu, R., and Joachimiak, A. (2005) Unpublished structure of xanthine phosphoribosyltransferase from *Bacillus subtilis*, coordinates deposited *Protein Data Bank ID 1Y0B.*
43. Gill, S. C., and von Hippel, P. H. (1989) Calculation of protein extinction coefficients from amino acid sequence data, *Anal. Biochem. 182*, 319−326.
44. Jordan, D. B., Bisaha, J. J., and Picollelli, M. A. (2000) Catalytic properties of dihydroorotate dehydrogenase from *Saccharomyces cerevisiae*: studies on pH, alternate substrates, and inhibitors, *Arch. Biochem. Biophys. 378*, 84−92.
45. Kraulis, P. J. (1991) MOLSCRIPT: A Program to Produce Both Detailed and Schematic Plots of Protein Structures, *J. Appl. Crystallogr. 24*, 946−950.
46. Merritt, E. A., and Bacon, D. J. (1997) Raster3D photorealistic molecular graphics, *Methods Enzymol. 277*, 505−524.
47. Ozturk, D., Dorfman, R. H., Scapin, G., Sacchettini, J. C., and Grubmeyer, C. (1995) Structure and function of *Salmonella typhimurium* orotate phosphoribosyltransferase: protein complementation reveals shared active sites, *Biochemistry 34*, 10764−10770.
48. Wallace, A. C., Laskowski, R. A., and Thornton, J. M. (1995) LIGPLOT: a program to generate schematic diagrams of protein-ligand interactions, *Protein Eng. 8*, 127−134.
49. Bhatia, M. B., Vititsky, A., and Grubmeyer, C. (1990) Kinetic mechanism of orotate phosphoribosyltransferase from *Salmonella typhimurium*, *Biochemistry 29*, 10480−10487.
50. Grabner, G. K., and Switzer, R. L. (2003) Kinetic studies of the uracil phosphoribosyltransferase reaction catalyzed by the *Bacillus subtilis* pyrimidine attenuation regulatory protein PyrR, *J. Biol. Chem. 278*, 6921−6927.
51. Elliott, W. H. (1959) in *Data for Biochemical Research* (Dawson, R. M. C., Elliott, D. C., Elliott, W. H., and Jones, K. M., Eds.) pp 66−75, Clarendon Press, Oxford.
52. Xu, Y., and Grubmeyer, C. (1998) Catalysis in human hypoxanthine-guanine phosphoribosyltransferase: Asp 137 acts as a general acid/base, *Biochemistry 37*, 4114−4124.
53. Schumacher, M. A., Bashor, C. J., Song, M. H., Otsu, K., Zhu, S., Parry, R. J., Ullman, B., and Brennan, R. G. (2002) The structural mechanism of GTP stabilized oligomerization and catalytic activation of the Toxoplasma gondii uracil phosphoribosyltransferase, *Proc. Natl. Acad. Sci. U.S.A. 99*, 78−83.
54. Henriksen, A., Aghajari, N., Jensen, K. F., and Gajhede, M. (1996) A flexible loop at the dimer interface is part of the active site of the adjacent monomer of *Escherichia coli* orotate phosphoribosyltransferase, *Biochemistry 35*, 3803−3809.
55. Sinha, S. C., and Smith, J. L. (2001) The PRT protein family, *Curr. Opin. Struct. Biol. 11*, 733−739.

BI060287Y